

Morphological Similarities between Single-Walled Nanotubes and Tubelike Structures of Polymers with Strong Adsorption Affinity to Nanowires

Thomas Vogel^{1,*}, Tali Mutat², Joan Adler² and Michael Bachmann¹

¹ Center for Simulational Physics, Department of Physics and Astronomy,
The University of Georgia, Athens, GA, 30602, USA.

² Department of Physics, Technion, Israel Institute of Technology, Haifa, 32000,
Israel.

Received 13 December 2011; Accepted (in revised version) 23 April 2012

Communicated by Leonardo Golubovic

Available online 8 October 2012

Abstract. In their tubelike phase, nanowire-adsorbed polymers exhibit strong structural similarities to morphologies known from single-walled carbon (hexagonal) and boron (triangular) nanotubes. Since boron/boron nitride tubes require some disorder for stability the triangular polymer tubes provide a closer analog to the carbon tubes. By means of computer simulations of both two and three dimensional versions of a coarse-grained bead-spring model for the polymers, we investigate their structural properties and make a detailed comparison with structures of carbon nanotubes.

AMS subject classifications: 82B80, 82D60, 82D80

PACS: 82.35.Gh, 05.10.Ln, 61.48.De

Key words: Polymers on surfaces, Monte Carlo methods, structure of carbon nanotubes, boron nanotubes.

1 Introduction

In a recent computational study, it could be shown that flexible polymers interacting with a wirelike substrate possess a barrellike phase [1]. Optimally packed, the monomers form a cylindrical polymer tube, reminiscent of a triangular lattice which wraps around the wire. Depending on the competition between steric constraints and monomer-substrate

*Corresponding author. *Email addresses:* thomasvogel@physast.uga.edu (T. Vogel), talimu@techunix.technion.ac.il (T. Mutat), phr76ja@techunix.technion.ac.il (J. Adler), bachmann@smsyslab.org (M. Bachmann)

attraction, other structural phases can also form. These phases were also found in previous, related studies of polymers interacting with nanocylinders [2, 3].

Tubelike structures formed by atoms or molecules possess interesting physical properties such as amazing mechanical stability, which make them potential candidates for nanotechnological applications. Recently, tin nanowires have been coated with atomic nanotube structures in order to stabilize them for conducting superconductivity experiments, i.e., protect them from shape fragmentation as well as from oxidation [4]. The understanding of the wetting behavior of atomic nanotubes with polymeric materials has been claimed to be the key to carbon nanotube-polymer composites [5]. Biological cells require a stable cytoskeleton which consists of tubelike myosin fibers.

The most prominent examples of tubes on atomistic scales are carbon nanotubes [6,7] which can be thought of as “rolled-up” and “zipped” sheets of graphene, sharing its hexagonal honeycomb lattice structure and sp^2 hybridized atoms [8–11]. Specifically, single-walled carbon nanotubes (SWCNTs) have been extensively studied on different levels of approximation. While nanotube models are typically based on continuum approximations, it has recently been shown that their atomistic nature is crucial for correct estimation of nanotube parameters [12, 13].

As well as carbon nanotubes, boron and boron nitride tubes have also been created [14] and modeled. A review of boron tube modeling is given in [15]. The salient differences between boron and carbon tubes are that the boron tubes form a triangular lattice structure (as do the polymer tubes) but the boron tubes appear to require either puckering, substitution with nitrogen or regular vacant sites for stability, unlike both polymer and carbon tubes. Thus the polymer tubes share one feature – the underlying lattice – with single-walled boron nanotubes (SWBNTs) and another – non-buckled, translationally invariant surfaces – with the carbon tubes.

From a formal point of view the hexagonal nanotube atomic lattice is dual [16] to the triangular lattice, suggesting there may be a deeper connection. This has been extensively explored for idealized single-walled boron nanotubes [15], but the buckling or regular vacancies in real boron tube structures complicate a precise modeling. The polymer tubes we investigate in this study are complete, unbuckled triangulations of single-walled tubes and thus we can directly adopt the theory introduced in [15] for idealized boron tubes to link our results for polymer tubes with known atomic boron and carbon nanotube structures.

This paper is structured as follows. The description of the hybrid polymer-wire model leading to monolayer polymer tube conformations for certain parameters, and a summary of our previous findings on those systems, is given in Section 2. In Section 3 we present details of typical nanotube configurations and quantify their characterization. Since the correct treatment of discrete tube structures is indispensable for our discussion and was introduced quite recently, we also review the polyhedral model for the description of ideal nanotubes in detail. In Sections 4 and 5 we will present a detailed discussion of our mappings and simulations based on Monte Carlo simulations in the full three dimensional space (Section 5.1). These simulations indicate that it is indeed adequate to

restrict the investigation to polymers on cylindrical surfaces (Section 5.2) in order to introduce a precise classification of polymer tubes. We show that while certain crucial differences are present, there is a deep similarity between atomistic nanotubes and polymer tubes. A summary of observations and conclusions will complete the paper.

2 Structural properties of polymer tubes

2.1 Polymer-wire model

For our study of polymer tubes, we employ a coarse-grained hybrid model of a flexible, elastic polymer interacting with an attractive stringlike nanowire. We found recently that such a system possesses a conformational phase, in which tubelike monolayer structures spontaneously form [1]. In our model, pairs of monomers interact via a truncated and shifted Lennard-Jones (LJ) potential

$$V_{\text{LJ}}^{\text{mod}}(r_{ij}) = V_{\text{LJ}}(\min(r_{ij}, r_c)) - V_{\text{LJ}}(r_c) \quad (2.1)$$

with the standard form of the LJ potential

$$V_{\text{LJ}}(r_{ij}) = 4\epsilon[(\sigma/r_{ij})^{12} - (\sigma/r_{ij})^6], \quad (2.2)$$

where r_{ij} denotes the distance between the i th and j th monomer. We set the respective intrinsic energy and length scales to $\epsilon = 1$ and $\sigma = 2^{-1/6}r_0$ with the minimum-potential distance $r_0 = 1$. The cutoff is chosen to be $r_c = 2.5\sigma$. Covalently bonded adjacent monomers in the linear polymer chain interact via the finitely extensible nonlinear elastic (FENE) potential, which has the form [17, 18]

$$V_{\text{FENE}}(r_{ii+1}) = -\frac{K}{2}R^2 \ln\{1 - [(r_{ii+1} - r_0)/R]^2\}. \quad (2.3)$$

Its minimum coincides, by construction, with r_0 and diverges for $r \rightarrow r_0 \pm R$. We set $R = 0.3$ and $K = 40$.

The interaction of the polymer with the wire is modeled by the potential

$$V_{\text{string}}(r_{\perp;i}) = \pi a \epsilon_f \left(\frac{63}{64} \frac{\sigma_f^{12}}{r_{\perp;i}^{11}} - \frac{3}{2} \frac{\sigma_f^6}{r_{\perp;i}^5} \right), \quad (2.4)$$

where σ_f and ϵ_f are the monomer-wire interaction parameters and $r_{\perp;i}$ is the distance of the i th monomer perpendicular to the wire. We scale the potential such that its minimum value is -1 at r_{\perp}^{min} for $\epsilon_f = 1$ and $\sigma_f = 1$, in which case $a \approx 0.528$; see also [19]. The effective thickness of the string, σ_f , is related to the minimum distance r_{\perp}^{min} of the monomer-wire potential via

$$r_{\perp}^{\text{min}}(\sigma_f) = (693/480)^{1/6} \sigma_f \approx 1.06 \sigma_f. \quad (2.5)$$

Eventually, the total energy of the polymer interacting with the wire is given by

$$E = \sum_{i,j=i+1}^N V_{\text{LJ}}^{\text{mod}}(r_{ij}) + \sum_{i=1}^{N-1} V_{\text{FENE}}(r_{ii+1}) + \sum_i^N V_{\text{string}}(r_{\perp,i}). \quad (2.6)$$

In order to identify structural properties of low-energy adsorbed polymer conformations, we employed stochastic minimization techniques based on generalized-ensemble Monte Carlo sampling strategies such as the energy-landscape paving method [20], multicanonical sampling [21], and the Wang-Landau method [22].

2.2 Structural phases of the polymer-wire system

In close analogy to a recent study of a bead-stick polymer interacting with a nanowire [1], the full spectrum of structural phases can be revealed. Depending on the wire attraction strength ϵ_f and its effective thickness σ_f , spherically globular or rather extended conformations dominate. Although in this paper we are interested in the tubelike structural phase of the polymer-wire system only, let us briefly review all phases identified. In Fig. 1, representative examples of low-energy conformations in the different phases are depicted.

If the value of ϵ_f is small enough that monomer-monomer contacts are energetically more favorable than contacts with the substrate, the lowest-energy conformations are compact spherical globules. Since the wire is always attractive, the number of monomer-substrate contacts is also maximized, such that the globular structures inclose the wire [phase “Gi” (globular inclosed), see Fig. 1(c)]. If, on the other hand, the length scale

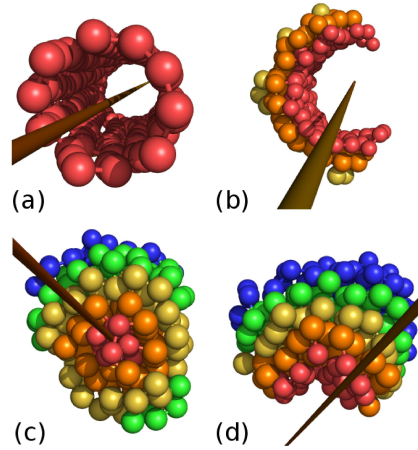


Figure 1: Exemplified images of representative low-energy conformations in the four structural phases (see text) of a polymer with 200 monomers interacting with an attractive nanowire. The parameter settings are: (a) $\epsilon_f=5.0$, $\sigma_f=1.5$ (in structural phase B), (b) $\epsilon_f=3.5$, $\sigma_f=2.5$ (C), (c) $\epsilon_f=2.0$, $\sigma_f=0.5$ (Gi), (d) $\epsilon_f=1.0$, $\sigma_f=1.5$ (Ge).

of the monomer-wire interaction exceeds the length scale of the pairwise LJ-interaction among two monomers, the wire is pushed outward and the globule is simply attached to the wire [this phase is called “Ge” (globular excluded), see Fig. 1(d)]. Starting from phase Ge and increasing the energy scale of the attraction to the wire, the morphology of conformations changes. The wire-attached spherically symmetric globules “melt” along the wire axis and reach what is called the “clamshell phase” C, see Fig. 1(b). The spherical morphology is broken and the polymer starts wrapping around the wire in order to increase the energetically favored contacts with the substrate.

If the string thickness is reduced below the corresponding threshold value, the clamshells turn to “barrels” and the structural phase B is reached. The same scenario occurs, when approaching from the Gi phase and passing the transition point, where the energy scale of the monomer-substrate attraction is sufficiently large compared to the intrinsic polymer energy scale of nonbonded LJ-interactions to allow for an increase of monomer-substrate contacts at the expense of monomer-monomer contacts. Since additional contacts with the wire can only be formed along the wire axis, the polymer forms compact tubelike structures in this phase, see Fig. 1(a).

For our discussion of similarities of the polymer-wire system with carbon nanotubes, we will refer below only to the monolayer polymer tube structures formed in phase B. Before embarking on the comparison of polymer tubes and carbon nanotubes, we briefly review relevant geometrical properties of SWCNTs.

3 Single-walled nanotubes

Nanotubes are typically considered as rolled-up planar atomic sheets. A single-walled carbon nanotube (SWCNT) is commonly pictured as a zipped monolayer graphene sheet (although, more detailed approaches exist [23]), crystallized on a hexagonal (honeycomb) lattice. All carbon atoms have the same distance from the tube axis and thus reside on a cylinder surface. In the original, conventional model, the SWCNT lattice was supposed to entirely cover a cylinder, thereby assuming curved hexagonal plates and bonds, neglecting the discrete nature of the lattice [11]. In a more realistic polyhedral decomposition approach, this is corrected by formulating constraints regarding C-C bond lengths and angles between them [15,24].

Single-walled boron nanotubes (SWBNTs) possess an underlying triangular lattice structure and have also been described by cylindrical mappings [15,25]. Energetically favored tube structures possess holes or are puckered, in which case the atoms do not lie on a surface of a single cylinder [26,27]. Other, non-regular structures, have also been considered in theoretical studies of SWBNTs [28].

The triangular single-walled polymer tube (SWPT) structures we find in the barrel phase of a polymer adsorbed at a nanowire exhibit strong similarities with ideal cylindrical SWBNTs. Thus, for its geometrical description the ideal polyhedral model for SWBNTs with equal bond lengths [25] can easily be adopted. Since the polymers tend

to form highly regular tube structures, they are interesting candidates for carbon nanocomposites of polymers and SWCNTs. For these reasons, it is instructive to discuss the relationship of SWCNTs and SWPTs in the following.

3.1 The conventional view on carbon nanotubes

In the unzipped, conventional representation, the chiral or wrapping vector \mathbf{C}_h pointing from any lattice site to its next copy (see Fig. 2) uniquely characterizes any SWCNT structure. The wrapping vector and the translational vector \mathbf{T} , perpendicular to \mathbf{C}_h , span the unit cell. It is convenient to introduce lattice vectors \mathbf{a}_1 and \mathbf{a}_2 (see Fig. 2), such that $\mathbf{C}_h = n\mathbf{a}_1 + m\mathbf{a}_2$ and $\mathbf{T} = [(n+2m)/d]\mathbf{a}_1 - [(2n+m)/d]\mathbf{a}_2$, where d is the greatest common divisor of $n+2m$ and $2n+m$. Hence, the two integers n and $m \leq n$, usually written in the vector form (n,m) , are sufficient to differentiate between SWCNT structures.

The wrapping orientation is defined by the characteristic wrapping or chiral angle θ between \mathbf{a}_1 and \mathbf{C}_h , i.e.,

$$\cos\theta_{\text{conv}}^{(n,m)} = (2n+m)/2\sqrt{n^2+m^2+nm}. \quad (3.1)$$

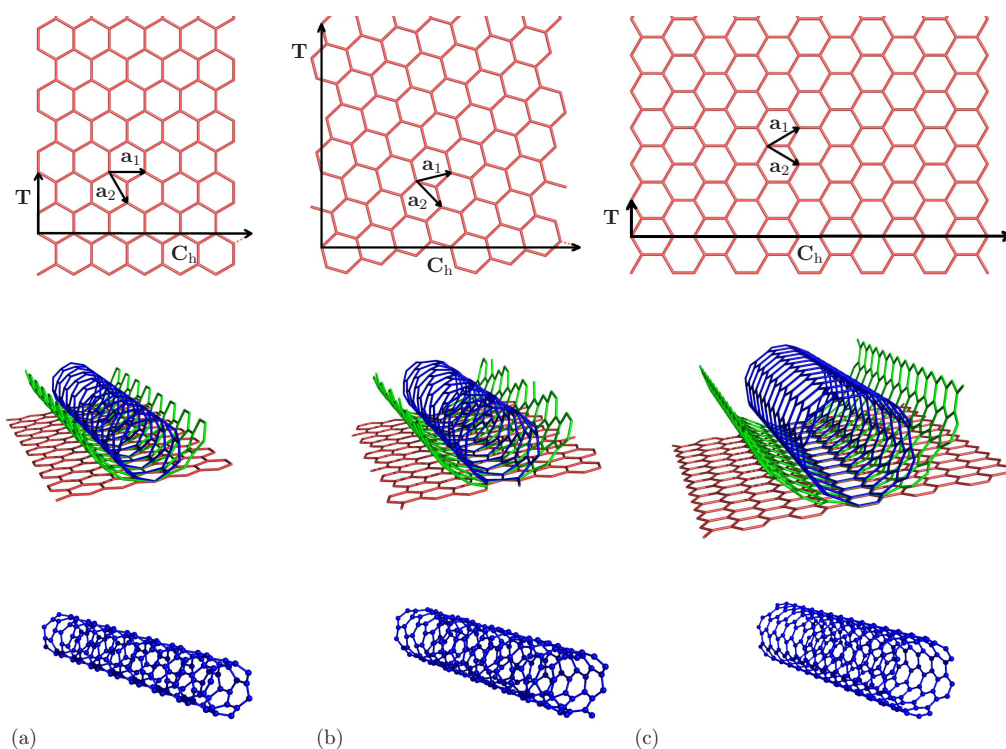


Figure 2: Examples of carbon nanotube structures: (a) zigzag (6,0), (b) chiral (6,2), and (c) armchair (6,6) conformation. In the top row, unzipped and unrolled planar representations are shown, the middle row illustrates the zipping and at the bottom, the actual tube structures are visualized.

Hence, θ can take values between 0 and 30° . The corresponding limiting tube conformations for a given value of n are usually called zigzag (for $m=0$) or armchair conformation (for $m=n$). In Fig. 2, different visualizations of $(6,m)$ zigzag, chiral, and armchair carbon nanotube structures are shown.

In this conventional approach [11], SWCNTs were assumed to be planar sheets of the (n,m) unit cell wrapped around a cylinder and continued along the central axis. Then, the length of \mathbf{C}_h corresponds to the circumference $L_{\text{conv}}^{(n,m)}$ of this cylinder. Since

$$|\mathbf{C}_h| = L_{\text{conv}}^{(n,m)} = \sqrt{3}l_{\text{CC}} \sqrt{n^2 + m^2 + nm}, \quad (3.2)$$

where $l_{\text{CC}} \approx 1.42\text{\AA}$ corresponds to the C–C bond length, the radius of the zipped SWCNT is given by

$$r_{\text{conv}}^{(n,m)} = L_{\text{conv}}^{(n,m)} / 2\pi. \quad (3.3)$$

In this simple cylindrical mapping, the bond length is not conserved and discrete curvature effects are not correctly taken into account. However, the flatter the surface, i.e., the larger n , the more accurate this estimate is.

For structural investigations of realistic SWCNTs, this difference is not of particular relevance. However, for our subsequent comparison and discussion of the relationship between triangular SWPTs and hexagonal SWCNT shapes, the (typically small) deviations must be taken into consideration, because the structural characterization on the basis of the (n,m) vector depends sensitively on this.

Assuming that the SWCNT forms under the constraints of conserved C–C bond lengths, which are not necessarily all equal [29], a discrete SWCNT model can be derived. The obtained geometric tube structures are in good correspondence with ab initio predictions and molecular dynamics relaxation [15, 30]. This model is also applicable to ultra-small nanotubes which resemble nanowires [31].

3.2 Polymer tubes and the polyhedral model for nanotubes

In the tube phase, polymers attracted by a thin wire form compact conformations. Because of the elasticity and flexibility of the polymer model considered here, monomers are optimally packed in a triangular arrangement. Unzipping such a polymer tube yields a regular triangular lattice, whose lattice vectors are identical with \mathbf{a}_1 and \mathbf{a}_2 introduced earlier for the definition of the wrapping vector \mathbf{C}_h of the SWCNTs. Consequently, the (n,m) notation for the characterization of SWCNTs can also be implemented to characterize the SWPTs.

The polymer tubes we find in the monolayer barrel phase of our polymer-nanowire adsorption model can be well described by the ideal boron nanotube model [15, 25], where all bonds are considered to have an identical length l_{BB} . This assumption corresponds well to the definitions of the length scales of bonded and nonbonded interactions in the FENE polymer model used in our study. Thus, the systems can easily be mapped onto each other by the replacement $l_{\text{BB}} \leftrightarrow r_0$. The polymers form monolayer tubes, if the

adsorption strength overcompensates optimal three-dimensional nearest-neighbor packing of the monomers. If the adsorption strength is reduced to the extent that intrinsic attraction becomes competitive, the topologically two-dimensional monolayer is given up in favor of a double-layer structure extending into the third dimension. The polymer undergoes a topological transition, but keeps a barrel-like form [1]. In the following, we only consider monolayer polymer tubes, as only in this conformational phase the analogy to carbon and (idealized) boron nanotubes is apparent.

Adopting the equations from the idealized boron nanotube model [25] and the chiral notation (n,m) from atomic nanotubes, the radius of an (n,m) polymer tube is given by

$$r_{\text{poly},\Delta}^{(n,m)} = \frac{r_0 \cos\theta^{(n,m)}}{2 \sin\psi^{(n,m)}}, \quad (3.4)$$

where r_0 is the equilibrium monomer-monomer distance [32] and the corrected wrapping angle $\theta^{(n,m)}$ is given by

$$\cos^2\theta^{(n,m)} = \frac{n(n+2m)\sin^2\psi^{(n,m)}}{(n+m)^2\sin^2\psi^{(n,m)} - m^2\sin^2(\psi^{(n,m)} + \zeta^{(n,m)})}. \quad (3.5)$$

The angles $\psi^{(n,m)}$ and $\zeta^{(n,m)} = (n\psi^{(n,m)} - \pi)/m$ are defined by projections of atom positions upon a circular slice perpendicular to the tube axis [25]. They are obtained by solving the transcendental equation

$$0 = (n^2 - m^2)\sin^2(\psi^{(n,m)} + \zeta^{(n,m)}) - n(n+2m)\sin^2\zeta^{(n,m)} + m(2n+m)\sin^2\psi^{(n,m)}. \quad (3.6)$$

See also Fig. 3 for definition of the angles ψ and θ .

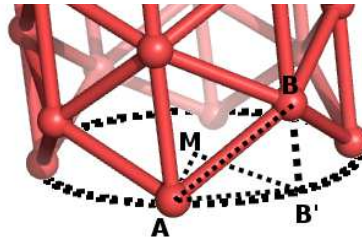


Figure 3: Definitions of the angles ψ and θ , shown exemplarily using a part of a $(4,4)$ SWPT. $2\psi = \angle(\mathbf{AMB}')$; $\theta = \angle(\mathbf{BAB}')$.

Analogously one can formulate equations for $\theta^{(n,m)}$ and $r_{\text{poly},\square}^{(n,m)}$ for the polyhedral model for carbon nanotubes with fixed bond lengths, crystallized in a curved honeycomb lattice structure. In fact, the wrapping angle $\theta^{(n,m)}$ for SWCNTs is identical to that of SWPTs and SWBNTs, respectively, as the base vectors $\mathbf{a}_{1,2}$ in the SWCNT structure correspond to the bond vectors in triangular tubes.

The calculation of the polyhedral radius is more challenging, as the honeycomb cell is not immune to shearing or tilting, as is a triangular lattice. Indeed, the curvature induced by the wrapping deforms the simple hexagonal cells, in contrast to triangular cells. The first-order correction of the polyhedral radius for SWCNTs is [30]:

$$r_{\text{poly},\square}^{(n,m)} = r_{\text{conv}}^{(n,m)} + \frac{\sqrt{3}\pi l_{\text{CC}} [4(n^2 + nm + m^2)^3 - 9n^2 m^2 (n+m)^2]}{64(n^2 + nm + m^2)^{7/2}} + \mathcal{O}(1/n^3). \quad (3.7)$$

For a concrete description of the limiting behavior of this model, we start with the observation that $\theta^{(n,m)} = \theta_{\text{conv}}^{(n,m)}$ (cf. Eqs. (3.1) and (3.5)) for the two special cases $n = m$ and $m = 0$, i.e., for (n,n) - and $(n,0)$ -tubes, the conventionally calculated wrapping angles of $\theta = 30^\circ$ and $\theta = 0^\circ$ are valid also in the polyhedral model. This leads to an intuitive interpretation for the radius of triangular $(n,0)$ -tubes. From the vanishing wrapping angle follows that there are bonds forming regular polygons with n edges in planes perpendicular to the tube orientation. Hence, the corresponding tube radius is the circumradius of such a polygon:

$$r_{\text{poly},\Delta}^{(n,0)} = \frac{r_0}{2\sin(\pi/n)}. \quad (3.8)$$

Analogously, the radius of triangular (n,n) -tubes can be directly calculated.

In this case, continuations of \mathbf{a}_1 or \mathbf{a}_2 , projected onto the wrapping vector (or, in the tube, the slice plane perpendicular to the tube axis), will form a regular polygon with $2n$ edges. Since the angle between the original vectors $\mathbf{a}_{1,2}$ and their projections, i.e., the wrapping vector θ , is $\pi/6$, the lengths of the projected vectors are shortened by the factor $\cos(\pi/6) = \sqrt{3}/2$. For the on-tube calculation of the bond length between two monomers, we make use of the fact that the projection angle in a triangular lattice does not change when zipping the planar sheet to a tube:

$$r_{\text{poly},\Delta}^{(n,n)} = \frac{\sqrt{3}r_0}{4\sin(\pi/2n)}. \quad (3.9)$$

Both, Eqs. (3.8) and (3.9), are of course covered by Eq. (3.4), as Eq. (3.6) implies $\psi = \pi/2n$ and $\psi = \pi/n$ for $(n,0)$ and (n,n) tubes, respectively.

Note that it is not possible to apply similar arguments to calculate the correct radii of $(n,0)$ and (n,n) SWCNTs, because the hexagon is not rigid, as the triangle is. Thus distances between the atoms in the hexagon change when bending. Indeed, for hexagonal honeycomb tubes (SWCNTs) one finds, when projecting bonds to planes perpendicular to the tube orientation, polygons with $3n$ and $2n$ edges for armchair and zigzag-tubes, respectively. But these polygons are not regular anymore, in the armchair case, and the lengths of the projections cannot be calculated in such a straightforward way, due to minimal deformations caused by the curvature. However, applying such approximations and corresponding generalizations to (n,m) tubes lead to the same qualitative results, such as the (n,m) sequence for increasing radii, as shown below, for example. Quantitative deviations from results of the polyhedral model are in the low per-mille range (not shown).

Generally, although the numerical differences of $r_{\text{conv}}^{(n,m)}$ (Eq. (3.3), with the respective scale) and $r_{\text{poly}}^{(n,m)}$ (Eqs. (3.4) and (3.7)) do not seem to be particularly striking, and may not be distinguished in practice, in particular at finite temperatures due to fluctuations of the bond lengths and the tube itself, the physical consequences are actually important to notice. Consider, for example, (7,0) and (5,3) SWCNTs. Using Eq. (3.3), both would share the same radius $r_{\text{conv}}^{(7,0)} = r_{\text{conv}}^{(5,3)} = \sqrt{3}l_{\text{CC}}\sqrt{7}/2\pi$ and could not be distinguished using this quantity. However, the structures of the corresponding tubes are completely different, and in consequence, physical, i.e., nanoelectronic, nanooptic and other material properties [11,33–35], are in general different as well. Hence, $r_{\text{conv}}^{(n,m)}$ is not suitable to parametrize SWCNTs, whereas $r_{\text{poly}}^{(n,m)}$ can uniquely be associated to any SWCNT structure. A more detailed numerical analysis of the deviations between the conventional and the polyhedral approach is given in [36].

However, for the following discussion of similarities of SWCNTs and SWPTs, significant precision is required and therefore it is necessary to take into account these differences.

4 Mapping between carbon nanotubes and polymer tubes

Since the triangular lattice formed by an unzipped SWPT is obtained from a Voronoi construction of the hexagonal lattice formed by the carbon atoms in an unzipped SWCNT, it is appealing to investigate the mapping between these different systems. This is not only mathematically interesting, but might also have technological consequences for the design of particularly stable polymer coated carbon nanotubes or other nanohybrid structures including SWCNTs and complex molecules [3, 5, 37–42].

However, as we have discussed in the previous section, it is necessary to examine geometrical considerations on the tube itself and not on its unzipped form. This is not trivial due to the curvature and discrete nature of those systems, which affects, for example, the bending angles between the respective carbon atoms or monomers such that they generally differ in the unzipped planar shape and in the tube structure.

Exemplified for $(4,m)$ tubes, Fig. 4 shows in various types of visualization the general construction principle of triangular polymer tubes out of honeycomb SWCNT structures. A monomer of the polymer chain is placed in the center of each “hexagonal” plaquette on the tube, i.e., at the position of the vertices of the associated Voronoi graph of the hexagonal lattice points in flat (unzipped) space, and then the monomer is shifted along the axis perpendicular to the tube axis to the correct distance $r_{\text{poly},\square}^{(n,m)}$ from the tube axis. Fig. 4 (b) and (c) enable one to sense the generally non-trivial geometrical structure of SWCNTs. In Fig. 4 (d) the helical aspect of the corresponding triangular tubes, to which we will return later, is emphasized.

The length scale in the triangular tube is obviously different from that in the SWCNT. The resulting scaling of bond lengths is of particular interest. Equivalently, one can ask

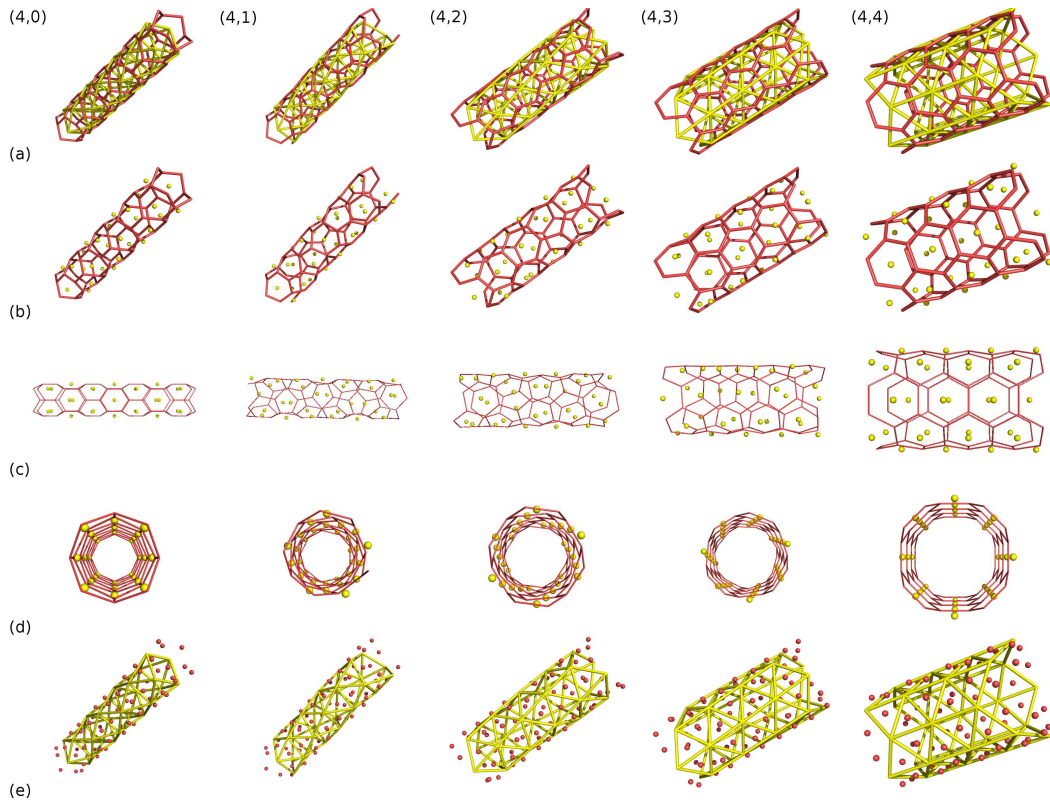


Figure 4: Different visualizations of $(4,m)$ nanotubes with (l. to r.) $0 \leq m \leq 4$. Hexagonal SWCNT (red online) and the corresponding ideal triangular tubes (yellow online) are shown from different viewpoints and combinations of lattice points (atomic positions) and edges (bonds). The data is the same for each column (m value) with all lattice points always shown, but edges only in some cases specifically (a) both, (b), (c) and (d) bonds of SWCNTs only and (e) bonds of triangular tubes only.

for the radius of an (n,m) polymer tube, with a monomer-monomer bond length scale r_0 equal to l_{CC} . As known, the scaling factor in the conventional planar representation is $a_{conv} = \sqrt{3}$ independently of n or m , which is hence the limiting case for $n \rightarrow \infty$ in the tube geometry. For small n and m ,

$$\frac{a_{poly}^{(n,m)}}{\sqrt{3}} := \frac{r_{poly,\square}^{(n,m)}(l_{CC})}{\sqrt{3}r_{poly,\triangle}^{(n,m)}(r_0=l_{CC})} \xrightarrow{n \rightarrow \infty} 1$$

is plotted in Fig. 5 (solid line, “+” symbols, left scale).

The influence of the first correction term to $r_{conv}^{(n,m)}$ in Eq. (3.7) is connected to this scaling. The term is also plotted in Fig. 5 (dashed line, “×” symbols, right scale) and can be considered to be an estimate of the error made by applying Eq. (3.3) for the calculation of the SWCNT radius. This error can be bigger than the differences between radii of two SWCNTs of different type [36].

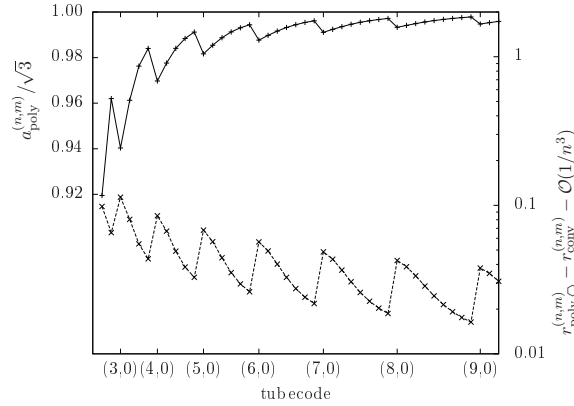


Figure 5: Solid graph, left scale: Normalized scaling of lengths in SWCNTs compared to SWPTs in the polyhedral model. The upper bound of the plot corresponds to the limiting value of $a_{\text{poly}}^{(n,m)} / \sqrt{3}$ for $n \rightarrow \infty$.

Dashed graph, right (logarithmic) scale: numerical value of the first order correction term to $r_{\text{conv}}^{(n,m)}$ in Eq. (3.7) for SWCNTs in the polyhedral model. The x axis is ordered with respect to increasing n and m , i.e., between two tics marked $(n,0)$ and $(n+1,0)$ tubes, all (n,m) tubes with increasing $0 < m \leq n$ are located.

5 Computer simulations of polymer tube structures

In the following, we present and discuss results from Monte Carlo minimizations of the bead-spring polymer-wire system introduced in Section 2 for strong wire attraction, such that the ground states form SWPTs. Compared to the model used in [1], we introduced extendible bonds and adjusted the equilibrium distance of the Lennard-Jones interactions such, that it coincides with the equilibrium length of the FENE bond potential. This simplifies the simulations and the bond-length flexibility limits, at this point, the occurrence of defects.

5.1 Simulation in the full conformational space

We perform simulations using generalized-ensemble Monte Carlo techniques [20–22] to search for low-energy configurations. We propose new structures through local updates of the Cartesian monomer coordinates, global spherical-cap updates [43], slithering snake moves, and bond-exchange moves [44].

The results of simulations with polymers of the length $N = 32$ are summarized in Table 1. In all our simulations, we set $\epsilon_f = 5.0$, i.e., we simulate structures in the monolayer barrel region 'B' [1]. The input to the simulation is σ_f , i.e., the effective thickness of the wire, is given in the first column. In the following columns, average values of measured local observables are shown. The tube radius r is, for example, measured as $r = \sum_{i=1}^N r_i / N$, with r_i being the perpendicular distance of the i th monomer from the center of the string. The small variance indicates that the monomers are located on a cylinder surface, in fact. Definitions of the characteristic angles ψ and θ , which are also measured

Table 1: Characteristics of polymer tubes formed by FENE-polymers adsorbed to a string in the polymer-wire model. The measured quantities are average values from local measurements at single monomers in the lowest-energy structures, see the text for details.

input σ_f	measured from lowest-energy state				calculated using polyhedral model		
	r	2ψ in $^\circ$	θ in $^\circ$	(n,m)	$r_{\text{poly},\Delta}^{(n,m)}$	$2\psi_{\text{poly},\Delta}^{(n,m)}$ in $^\circ$	$\theta_{\text{poly},\Delta}^{(n,m)}$ in $^\circ$
0.47	0.504 ± 0.002	131.9 ± 2.6	19.1 ± 0.7	(2,1)	0.51962	131.8	18.43
0.53	0.566 ± 0.002	120.0 ± 0.8	0.0 ± 0.4	(3,0)	0.57735	120.0	0.00
0.56	0.597 ± 0.002	89.9 ± 0.8	30.7 ± 0.5	(2,2)	0.61237	90.0	30.0
0.61	0.646 ± 0.002	98.0 ± 0.9	13.3 ± 0.6	(3,1)	0.64526	97.7	13.6
0.65	0.692 ± 0.002	90.0 ± 0.4	0.0 ± 0.3	(4,0)	0.70711	90.0	0.00
0.69	0.732 ± 0.003	76.5 ± 0.6	23.5 ± 0.3	(3,2)	0.74313	76.3	23.3
0.74	0.783 ± 0.003	77.4 ± 0.5	10.6 ± 0.4	(4,1)	0.78561	77.4	10.7
0.78	0.831 ± 0.003	72.1 ± 0.6	0.0 ± 0.4	(5,0)	0.85065	72.0	0.00
0.81	0.858 ± 0.003	60.0 ± 0.3	30.1 ± 0.5	(3,3)	0.86603	60.0	30.0
0.83	0.880 ± 0.004	64.7 ± 0.4	19.0 ± 0.4	(4,2)	0.88462	64.6	19.0
0.88	0.932 ± 0.004	64.0 ± 0.3	8.8 ± 0.4	(5,1)	0.93259	64.0	8.84

locally at each monomer and then averaged, are given in Fig. 3. We convinced ourselves by simulating all structures at different chain lengths that the results are independent of the actual choice of N . By applying the polyhedral model for triangular tubes, an (n,m) tube code, given in the fifth column, can uniquely be assigned to each pair (ψ, θ) . Finally, in the last three columns, the corresponding calculated geometric observables using the polyhedral model are given, which agree perfectly with the measured ones. The radius does not match exactly though, which is due to the fact that we did not use the calculated values from the model as input for the simulations, but σ_f in steps of 0.01 to avoid any potential bias. However, the flexibility of the bonds allows the compensation of these small deviations without causing defects in the ground-state structures. We will comment on that in more detail in the next section. After all, we find, that the polyhedral model for boron nanotubes [15] is suitable to describe the completely adsorbed polymer ground-state structures of a simple polymer-wire model. Some example structures are visualized in Fig. 6.

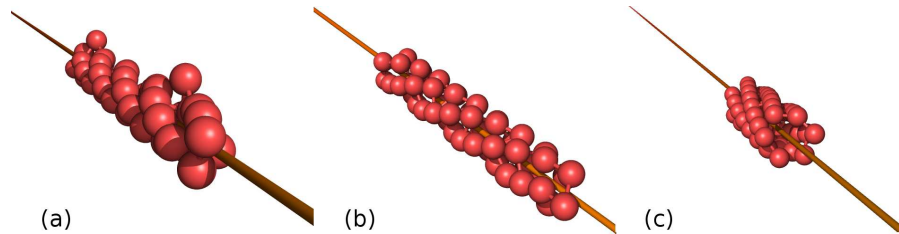


Figure 6: Low-energy tube structures of the simulated polymer-wire model. The structures were found for different σ_f (cp. Table 1): (a) $\sigma_f = 0.47$. Slightly excited state, two monomers do not belong to the monolayer around the wire. The monomers in that closest layer form a (2,1) tube. (b) $\sigma_f = 0.61$. Putative ground-state forming a (3,1) tube around the wire. (c) $\sigma_f = 0.83$. Putative ground-state forming a (4,2) tube. All shown polymers consist of $N = 48$ monomers.

5.2 Simulations on a cylinder surface

Since we find in the perfect monolayer tube conformations all monomers at the same distance from the tube axis, i.e., fluctuations of the local radius of the monolayer tubes were in fact vanishing, it is useful to directly simulate the polymer on a cylinder surface with fixed radius r . Following this idea, we randomly initialize conformations in such a way that each monomer has the same distance r from the string. We propose new structures by local updates and slithering snake moves in cylindrical coordinates keeping r untouched. This reduces the conformational space significantly and will allow us to refine our results shown above and determine, for example, intervals of radii with stable ground-state conformations. Furthermore, longer chains and hence larger tube radii could be studied. Finally, as an outlook to subsequent work, defects can be investigated in detail. See Section 5.3 below, for an example.

Simulations were now performed for different r values in the range $r \in [0.425, \dots, 1.424]$ independently, with a step width of about 0.01. The lengths of the simulated polymer chains ranged from $N = 32$ to 200. The results presented below also did not depend on the actual number of monomers N .

As mentioned above, we are looking for ground states in order to find a classification scheme for polymer nanotubes that depends on their radius, analogously to that of the carbon nanotubes. Indeed, this can be reduced to the measurement of the characteristic angles ψ and θ of such lowest-energy polymer tubes, which we measure as described above, depending on the given radius. For defect-free conformations, this can then be related to known observables of SWCNTs.

Table 2 summarizes results from this part of our computational study, and in Fig. 7 we visualize some of the putative ground-state structures we found that belong to different chirality classes. The illustrated structures are marked in Table 2 with an asterisk. The

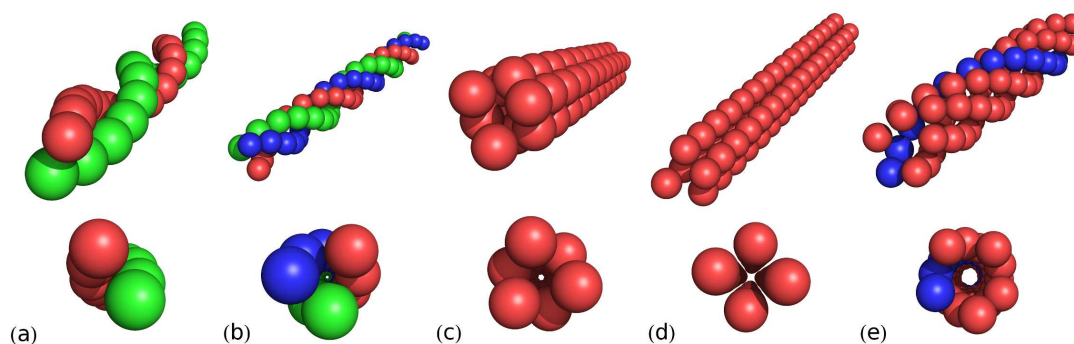


Figure 7: Putative ground-state structures of the polymer model restricted to a cylinder surface. The structures were found at different tube radii and belong to different chirality classes. (a) Double-helix; (b) Triple-helix, (2,1) tube; (c) (3,0) tube; (d) (2,2) tube; (e) 5-helix, (4,1) tube. Every picture shows a single polymer, whereas just the monomer positions are shown and not the bonds between consecutive monomers. Different colors were used to mark imaginary helical strands. The top row shows a perspective view on the structures, the bottom row a top view.

Table 2: Characteristics of lowest-energy states of simulated extendible polymers on cylindrical surfaces with radius r . The given angles are, as before, average values based on local measurements. See text for a detailed description. Structure types marked with an “*” are visualized in Fig. 7.

Calculated polyhedral polymer tube			Simulation on Cylinder surface (“2D”)			Corresponding SWCNT	
(n,m)	$r_{\text{poly},\Delta}^{(n,m)}$	2ψ in $^\circ$	input r	output (Lowest-energy state) type	2ψ in $^\circ$	θ in $^\circ$	θ in $^\circ$ type
(1,1)			0.425	(1,1)	181 ± 6	30.4 ± 0.5	30.00 (1,1)
			0.436...0.447	Double-helix*		$(29.2 \dots 27.6) \pm 0.7$	
(2,0)			0.457...0.466	(2,0)	180 ± 2	0.0 ± 1.2	0.00 (2,0)
(2,1)	0.51962	131.810	0.477...0.532	Triple-helix*	132 ± 2	$(20.8 \dots 17.5) \pm 1.0$	18.43 (2,1)
(3,0)	0.57735	120.000	0.553...0.574	(3,0)*	120 ± 0.8	0.0 ± 0.5	0.00 (3,0)
(2,2)	0.61237	90.0000	0.585...0.617	(2,2)*	90 ± 1	$(31.3 \dots 29.6) \pm 0.3$	30.00 (2,2)
(3,1)	0.64526	97.7431	0.627...0.670	4-helix	98 ± 1	$(13.9 \dots 12.6) \pm 0.7$	13.57 (3,1)
(4,0)	0.70711	90.0000	0.680...0.712	(4,0)	90.0 ± 0.7	0.0 ± 0.5	0.00 (4,0)
(3,2)	0.74313	76.3120	0.723...0.755	5-helix	76.4 ± 0.7	$(23.8 \dots 22.7) \pm 0.4$	23.33 (3,2)
(4,1)	0.78561	77.4148	0.765...0.808	5-helix*	77.5 ± 0.7	$(11.0 \dots 10.2) \pm 0.6$	10.72 (4,1)
(5,0)	0.85065	72.0000	0.819...0.851	(5,0)	72.0 ± 0.7	0.0 ± 0.6	0.00 (5,0)
(3,3)	0.86603	60.0000	0.861	(3,3)	60.0 ± 0.5	29.9 ± 0.4	30.00 (3,3)
(4,2)	0.88462	64.6055	0.872...0.904	6-helix	64.7 ± 0.9	$(19.2 \dots 18.3) \pm 0.5$	19.01 (4,2)
(5,1)	0.93259	63.9796	0.914...0.957	6-helix	64.0 ± 0.8	$(9.0 \dots 8.4) \pm 0.6$	8.84 (5,1)
(6,0)	1.00000	60.0000	0.967...	(6,0)	60.0 ± 0.6	0.0 ± 0.5	0.00 (6,0)
(4,3)	1.00188	53.6574	...1.021	7-helix	53.8 ± 0.6	26.2 ± 0.7	25.26 (4,3)
(5,2)	1.03116	55.5587	1.031...1.052	7-helix	55.5 ± 0.6	$(15.9 \dots 15.5) \pm 0.6$	16.02 (5,2)
(6,1)	1.08319	54.4683	1.063...1.106	7-helix	54.5 ± 0.6	$(7.6 \dots 7.2) \pm 0.5$	7.52 (6,1)
(4,4)	1.13152	45.0000	1.106...1.127	(4,4)	45.0 ± 0.5	$(30.3 \dots 30.0) \pm 0.5$	30.00 (4,4)
(5,3)	1.14441	47.8827	1.138	8-helix	47.9 ± 0.3	21.7 ± 0.4	21.75 (5,3)
(7,0)	1.15238	51.4286	1.148...1.169	(7,0)	51.4 ± 0.4	0.0 ± 0.6	0.00 (7,0)
(6,2)	1.18076	48.5578	1.169...1.201	8-helix	48.6 ± 0.5	$(13.9 \dots 13.4) \pm 0.5$	13.83 (6,2)
(7,1)	1.23600	47.3936	1.212...1.254	8-helix	47.4 ± 0.4	$(6.7 \dots 6.4) \pm 0.5$	6.54 (7,1)
(5,4)	1.26887	41.3657	1.244...1.276	9-helix	41.3 ± 0.3	$(26.8 \dots 26.0) \pm 0.6$	26.32 (5,4)
(6,3)	1.29090	42.9481	1.286	9-helix	42.9 ± 0.3	19.0 ± 0.5	19.07 (6,3)
(8,0)	1.30656	45.0000	1.297...1.318	(8,0)	45.0 ± 0.4	0.0 ± 0.6	0.00 (8,0)
(7,2)	1.33242	43.0405	1.318...1.361	9-helix	43.0 ± 0.5	$(12.2 \dots 11.8) \pm 0.6$	12.17 (7,2)
(8,1)	1.39027	41.9316	1.371...1.424	9-helix	41.9 ± 0.5	$(5.8 \dots 5.6) \pm 0.8$	5.79 (8,1)

first column shows an (n,m) tube code, the second and third column the corresponding calculated radius $r_{\text{poly},\Delta}^{(n,m)}$ and the angle ψ in the polyhedral model for triangular nanotubes (cf. Eqs. (3.4) and (3.6)). The rows are ordered with respect to increasing values of $r_{\text{poly},\Delta}^{(n,m)}$. In the fourth column, the input radius is given. Since transitions between different chiralities are not continuous, we give an interval of radii, for which the lowest-energy structures of the polymer fall into the same chirality class, which is given in the fifth column. By $(n+m)$ -helix we denote structures which can be considered to be composed of $n+m$ virtual, interwoven chains of monomers with a helical wrapping, see Fig. 7 for further clarification. The average values of the angles ψ and θ measured in the lowest-energy conformations are listed next to them. In the last two columns, known wrapping angles from SWCNTs could be uniquely assigned to the results from our SWPT simulations along with the corresponding SWCNT types.

5.3 Reproducing SWCNT sequences of chirality

If one sorts SWCNTs with respect to their radii, a specific sequence of chiralities is found. This sequence is exactly reproduced by polymer monolayer tubes, i.e., we can confirm the assumed correlation between SWCNTs and SWPTs [1]. In Table 2, we also compare the radii of (n,m) polymer tubes inserted into the simulations (column 4) with the exact values obtained from Eq. (3.4) (column 2), as well as with the characteristic angles ψ and θ (columns 3 vs. 6 and 7 vs. 8). Our simulation results agree perfectly with the predictions from the respective polyhedral model [25] and the high accuracy allow for the identification of the chiralities of the polymer tubes. Nonetheless, there are certain regions of radii, where the difference of radii between different tube types is extremely small. Within these regions, it is particularly challenging to resolve explicitly different chiralities (see the “plateaus” in Fig. 5 in [36]). In Table 2, results for (6,0) and (4,3) tubes are therefore listed in the same row. Their radii in the polyhedral model differs by less than 0.2%, which is reflected accordingly in our results. Regarding the wrapping angles, we could hence reproduce exactly the characteristic sequence for SWCNTs. Together with the considerations about the scaling of lengths between SWCNTs (cf. Fig. 5) this is the link between ideal SWCNTs and SWPTs.

We would like to emphasize that this accuracy is essential as one would not have been able to draw these detailed conclusions using the conventional approach (Eq. (3.3)) for the radius calculation. The polymer model with slightly different parameters that was used in [1] already yielded the correct trends of the present results, but only the flexible bond-length model allowed us to study the details precisely and quantitatively correct. In this case, we find transitions at the interfaces between two structural regions. We observe in the ensemble of low-energy states “competing” conformations, i.e., different tube types with very similar ground state energies and tubes with defects or internal interfaces between regions belonging to different chirality classes, see Fig. 8 for examples.

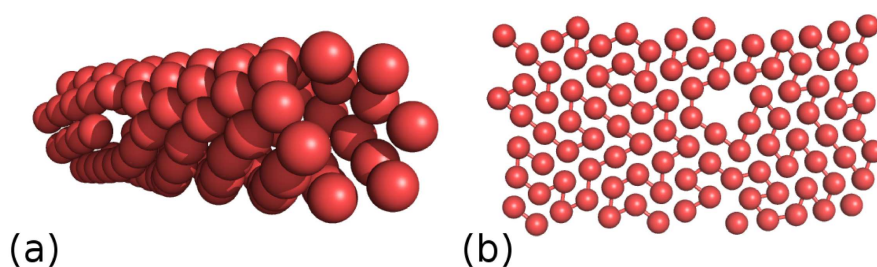


Figure 8: Low energy state with a defect and two regions with different wrappings. The radius of the tube is $r_{\text{input}} \approx 1.11$, the competing substructures correspond to (6,1)- and (5,3)-tubes. In (b) the conformation is shown in an unzipped view for clarity.

5.4 The link to the internal structure of 'phase B'

Actually, the intriguing monolayer polymer structures we found in our previous study [1] for strong wire adsorption, and which we summarized under the name 'barrel (B) phase', made us think about a possible link to single-walled carbon nanotubes and were the motivation for the present study. Beside the systematic presentation of the results above, let us therefore comment on some actual structures we found earlier.

At $\sigma_f = 0.647$, we found in a monolayer polymer conformation consisting of two competing substructures with different chirality and a defect at the interface between both substructures (see Fig. 9 (a)) [1]. One region forms a (2,2) tube, the other is a 4-helix with a measured mean wrapping angle of $\theta = 14 \pm 4$, which corresponds to a (3,1) tube. These observations fit in perfectly with the results presented above in Table 2. Both structures are neighbors in the radius-ordered sequence of tube structures. Slight deviations of the value of the radius and the larger error of the mean wrapping angle trace back to the fact that we originally used a slightly different polymer model with fixed bond length (sticks instead of elastic bonds) where the optimal distance between two nonbonded monomers was slightly larger than the bond length. However, on the other hand, this indicates that our results are of general character and do not depend on certain details of the implemented polymer model. Another conformation found in the earlier study was the, somewhat artificial, (1,1) tube at $\sigma_f = 0.4$ (see Fig. 9 (b)). Again, this was confirmed exactly by the present study and fits into the general scheme as presented here.

Finally, let us look at conformations with larger radius of $r \approx 1.7$, as shown in Fig. 9 (c). There, we found a 12-helix with chiral angle of $20 \pm 1^\circ$, which can now be assigned to a (8,4) tube (not listed in Table 2, but calculations lead to $\theta^{(8,4)} = 19.1$ and $r_{\text{poly},\Delta}^{(8,4)} = 1.71$). However, we also found in that region a strong competition between conformations with different structures as well as conformations composed of different substructures,

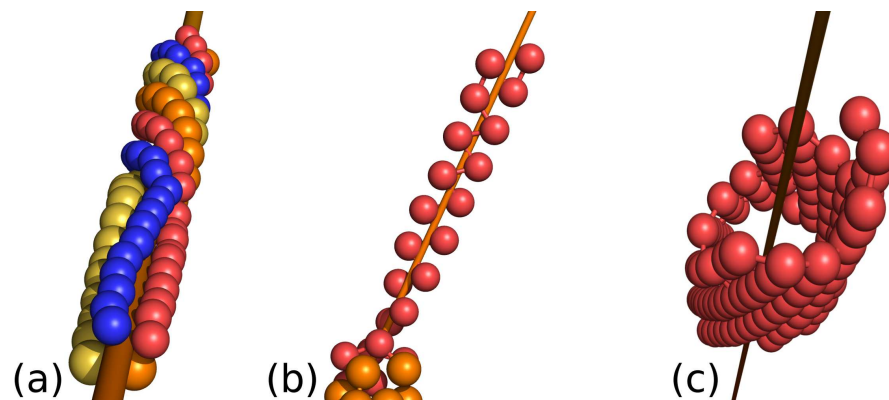


Figure 9: Monolayer polymer tubes in the barrel phase B for strong wire adsorption. (a) $\sigma_f = 0.65$, (b) $\sigma_f = 0.40$, and (c) $\sigma_f = 1.57$. Different colors or shadings shall facilitate the perception only, data taken from study presented in [1].

as shown for example in Figs. 1 and 4 in [45]. We find for example regions which can be explained to be parts of (7,5) tubes (not in Table 2, $\theta^{(7,5)} = 24.5$, $r_{\text{poly},\Delta}^{(7,5)} = 1.68$). This structure forms also a 12-helix, but with just slightly different wrapping angle compared to (8,4). Finally, we find among those structures (10,1) tubes ($\theta^{(10,1)} = 4.7$, $r_{\text{poly},\Delta}^{(10,1)} = 1.70$) forming 11-helices. Note the small differences between $r_{\text{poly},\Delta}^{(8,4)}$, $r_{\text{poly},\Delta}^{(10,1)}$ and $r_{\text{poly},\Delta}^{(7,5)}$.

6 Summary

In this study, we have investigated the relationship between single-walled carbon nanotubes and the tube phase of a bead-spring polymer model attracted by a thin wire. In fact, we found surprisingly clear geometrical similarities between these different materials. We could only obtain our results by taking into account the discreteness and curvature effects in the mathematical description of the geometrical properties of nanotubes. Hence, we provide an example for the necessity of applying accurate discrete models, rather than continuous approximations, in computational studies of nanotubes.

To strengthen our theoretical considerations on the link between carbon nanotubes and polymer nanotubes, we employed numerical optimization procedures to construct lowest-energy polymer conformations for given attraction length scales of the wire (or, equivalently, given polymer tube radii). Comparing those conformations based on a triangular lattice, with carbon nanotubes based on a hexagonal honeycomb lattice, we found that both share the same chirality sequence and we show how the length scales are connected. We addressed the problem of competing substructures leading to defects in non-ideal structures, which definitely merits further investigation.

The perfect structural coincidence between atomic nanotubes and polymer tubes explains the internal structure of the barrel phase of polymers adsorbed at nanowires. It is also a good starting point for the further systematic investigation of hybrid systems of polymers and single-walled carbon nanotubes, which might be of technological interest for controlling, e.g., physical properties of polymer-coated nanotubes. We have also presented further evidence, that helical conformations are intrinsic natural structures in simple polymer models [46].

Our key result of the universal nature of the sequence of conformations in nanotubes and polymer tubes has developed from a series of simulations. Such extensive 3d simulations have only recently become possible, and the situation is reminiscent of the discoveries in the seventies and early eighties as the picture of universality in critical phenomena emerged from the early numerical results of series expansions and simulations, and a very few experiments. With current and future computer power, the two directions mentioned above, namely the exploration of defective structures and the study of hybrid systems should lead into interesting theoretical and practical directions in polymer research and nanotechnology.

Acknowledgments

The authors would like to thank P. Pine and S. Srebnik from the Technion Haifa, for valuable discussions on nanotubes and adsorption of polymers at nanotubes. This project was in part supported by the Jülich/Aachen/Haifa Umbrella program under Grants No. SIM6 and No. HPC.2. Supercomputer time was provided by the Forschungszentrum Jülich under Projects No. jiff39 and No. jiff43.

References

- [1] T. Vogel and M. Bachmann, *Phys. Rev. Lett.* 104, 198302 (2010).
- [2] A. Milchev and K. Binder, *J. Chem. Phys.* 117, 6852 (2002).
- [3] I. Gurevitch and S. Srebnik, *Chem. Phys. Lett.* 444, 96 (2007); *J. Chem. Phys.* 128, 144901 (2008); S. Srebnik, *J. Polym. Sci. B: Polym. Phys.* 46, 2711 (2008).
- [4] N. Tombros, L. Buit, I. Arfaoui, T. Tsoufis, D. Gournis, P. N. Trikalitis, S. J. van der Molen, P. Rudolf, and B. J. van Wees, *Nano Lett.* 8, 3060 (2008).
- [5] M. Q. Tran, J. T. Cabral, M. S. P. Shaffer, and A. Bismarck, *Nano Lett.* 8, 2744 (2008).
- [6] S. Iijima, *Nature* 56, 354 (1991).
- [7] J.-C. Charlier, X. Blase, and S. Roche, *Rev. Mod. Phys.* 79, 677 (2007).
- [8] J. W. G. Wilder, L. C. Venema, A. G. Rinzler, R. E. Smalley, and C. Dekker, *Nature* 391, 59 (1998); T. W. Odom, J.-L. Huang, P. Kim, and C. M. Lieber, *ibid.* 391, 62 (1998).
- [9] M. Gao, L. Dai, and G. G. Wallace, *Electroanalysis* 15, 1089 (2003); T. Hasan, Z. Sun, F. Wang, F. Bonaccorso, P. H. Tan, A. G. Rozhin, and A. C. Ferrari, *Adv. Mater.* 21, 3874 (2009).
- [10] L. Valentini, J. Biagiotti, J. M. Kenny, and S. Santucci, *J. Appl. Polym. Sci.* 87, 708 (2002); L. Valentini, J. Biagiotti, M. A. López-Manchado, S. Santucci, and J. M. Kenny, *Polym. Eng. Sci.* 44, 303 (2004).
- [11] *Carbon Nanotubes: Synthesis, Structure, Properties, and Applications, Topics in Applied Physics, Vol. 80*, edited by M. S. Dresselhaus, G. Dresselhaus, and P. Avouris (Springer, Berlin, 2001).
- [12] Y. Huang, J. Wu, and K. C. Hwang, *Phys. Rev. B* 74, 245413 (2006).
- [13] P. Pine, Y. Yaish, and J. Adler, *Phys. Rev. B* 83, 155410 (2011).
- [14] D. Ciuparu, R. F. Klie, Y. Zhu, and L. Pfefferle, *J. Phys. Chem. B* 108, 3967 (2004).
- [15] R. K. F. Lee, B. J. Cox, and J. M. Hill, *Nanoscale* 2, 859 (2010).
- [16] J. W. Essam, *Phase Transitions and Critical Phenomena, Vol. 2*, edited by C. Domb and M. S. Green (Academic Press, New York, 1972).
- [17] R. B. Bird, C. F. Curtiss, R. C. Armstrong, and O. Hassager, *Dynamics of Polymeric Liquids, 2nd ed., 2 vols.* (Wiley, New York, 1987).
- [18] A. Milchev, A. Bhattacharaya, and K. Binder, *Macromolecules* 34, 1881 (2001).
- [19] T. Vogel and M. Bachmann, *Comp. Phys. Comm.* 182, 1928 (2011).
- [20] U. H. E. Hansmann and L. T. Wille, *Phys. Rev. Lett.* 88, 068105 (2002).
- [21] B. A. Berg and T. Neuhaus, *Phys. Lett. B* 267, 249 (1991); *Phys. Rev. Lett.* 68, 9 (1992).
- [22] F. Wang and D. P. Landau, *Phys. Rev. Lett.* 86, 2050 (2001).
- [23] J. Berashevich and T. Chakraborty, *Phys. Rev. B* 83, 195442 (2011).
- [24] R. K. F. Lee, B. J. Cox, and J. M. Hill, *J. Phys. Chem. C* 113, 19794 (2009).
- [25] R. K. F. Lee, B. J. Cox, and J. M. Hill, *J. Phys. A* 42, 065204 (2009).
- [26] J. Kunstmann and A. Quandt, *Chem. Phys. Lett.* 402, 21 (2005).

- [27] F.-Y. Tian, Y.-X. Wang, V. C. Lo, and J. Sheng, *Appl. Phys. Lett.* 96, 131901 (2010).
- [28] J. Wang, Y. Liu, and Y.-C. Li, *ChemPhysChem* 10, 3119 (2009).
- [29] M. F. Budyka, T. S. Zyubina, A. G. Ryabenko, S. H. Lin, and A. M. Mebel, *Chem. Phys. Lett.* 407, 266 (2005).
- [30] B. J. Cox and J. M. Hill, *Carbon* 45, 1453 (2007).
- [31] B. J. Cox and J. M. Hill, *Carbon* 46, 706 (2008).
- [32] In analogy to the length l_{CC} introduced for the C–C bond length in SWCNTs. For $n \rightarrow \infty$, $\sqrt{3}l_{CC} = r_0$ (cf. also Eq. (3.2)) for tubes with equal radii. The scaling between the lengths in triangular and honeycomb tubes for finite n will be discussed below.
- [33] J. Bernholc, D. Brenner, M. Buongiorno Nardelli, V. Meunier, and C. Roland, *Annu. Rev. Mater. Res.* 32, 347 (2002).
- [34] P. Kim and C. M. Lieber, *Science* 286, 2148 (1999).
- [35] M.S. Dresselhaus, G. Dresselhaus, and A. Jorio, *Annu. Rev. Mater. Res.* 34, 247 (2004).
- [36] T. Vogel, T. Mutat, J. Adler, and M. Bachmann, *Phys. Procedia* 15, 87 (2011).
- [37] M. in het Panhuis, A. Maiti, A. B. Dalton, A. van den Noort, J. N. Coleman, B. McCarthy, and W. J. Blau, *J. Phys. Chem. B* 107, 478 (2003).
- [38] C. Ehli, G. M. A. Rahman, N. Jux, D. Balbinot, D. M. Guldi, F. Paolucci, M. Marcaccio, D. Paolucci, M. Melle-Franco, F. Zerbetto, S. Campidelli, and M. Prato, *J. Am. Chem. Soc.* 128, 11222 (2006).
- [39] C. Ehli, C. Oelsner, D. M. Guldi, A. Mateo-Alonso, M. Prato, C. Schmidt, C. Backes, F. Hauke, and A. Hirsch, *Nat. Chem.* 1, 243 (2009).
- [40] C. Caddeo, C. Melis, L. Colombo, and A. Mattoni, *J. Phys. Chem. C* 114, 21109 (2010).
- [41] S. S. Tallury and M. A. Pasquinelli, *J. Phys. Chem. B* 114, 4122 (2010).
- [42] M. Gao, L. Dai, and G. Wallace, *Electroanalysis* 15, 1089 (2003).
- [43] M. Bachmann, H. Arkin, and W. Janke, *Phys. Rev. E* 71, 031906 (2005).
- [44] S. Schnabel, W. Janke, and M. Bachmann, *J. Comput. Phys.* 230, 4454 (2011).
- [45] T. Vogel and M. Bachmann, *Phys. Procedia* 4, 161 (2010).
- [46] T. Vogel, T. Neuhaus, M. Bachmann, and W. Janke, *EPJ E* 30, 7 (2009).